

Sterilizable Gels from Thermoresponsive Block Copolymer Worms

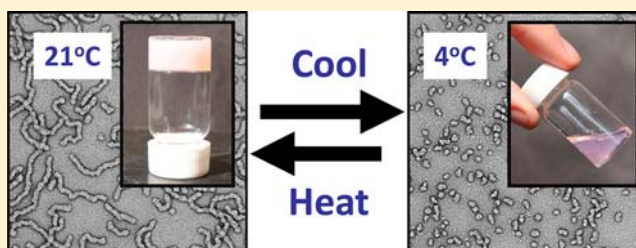
Adam Blanz,[†] Robert Verber,[†] Oleksandr O. Mykhaylyk,[†] Anthony J. Ryan,[†] Jason Z. Heath,[‡] C. W. Ian Douglas,[‡] and Steven P. Armes^{*,†}

[†]Department of Chemistry, The University of Sheffield, Dainton Building, Brook Hill, Sheffield S3 7HF, U.K.

[‡]Department of Oral Pathology, School of Clinical Dentistry, University of Sheffield, Claremont Crescent, Sheffield S10 2TA, U.K.

Supporting Information

ABSTRACT: Biocompatible hydrogels have many applications, ranging from contact lenses to tissue engineering scaffolds. In most cases, rigorous sterilization is essential. Herein we show that a biocompatible diblock copolymer forms wormlike micelles via polymerization-induced self-assembly in aqueous solution. At a copolymer concentration of 10.0 w/w %, interworm entanglements lead to the formation of a free-standing physical hydrogel at 21 °C. Gel dissolution occurs on cooling to 4 °C due to an unusual worm-to-sphere order–order transition, as confirmed by rheology, electron microscopy, variable temperature ¹H NMR spectroscopy, and scattering studies. Moreover, this thermo-reversible behavior allows the facile preparation of sterile gels, since ultrafiltration of the diblock copolymer nanoparticles in their low-viscosity spherical form at 4 °C efficiently removes micrometer-sized bacteria; regelation occurs at 21 °C as the copolymer chains regain their wormlike morphology. Biocompatibility tests indicate good cell viabilities for these worm gels, which suggest potential biomedical applications.



INTRODUCTION

Biocompatible hydrogels containing up to 99% water can be constructed using either synthetic or naturally occurring building blocks.^{1,2} They have numerous biomedical applications, such as soft contact lenses,³ tissue engineering scaffolds,⁴ protein purification and molecular weight determination,⁵ or drug delivery.⁶ Chemical gels are readily formed by introducing covalent cross-links within the matrix, whereas physical gels typically comprise extended networks formed from supramolecular assemblies. A range of either small molecule or polymeric nanostructures can be used to generate free-standing physical hydrogels. There are many literature examples of supramolecular gels based on either surfactants⁷ or oligopeptides.^{8,9} Stimulus-responsive reversible gelation based on either a pH switch or a change in temperature is also well-known for such small molecules.^{2,10–14} It is well-known that AB diblock copolymers can form ordered micellar gels at relatively high concentrations (usually >20 w/w %).¹⁵ ABA triblock copolymers can also form micellar gel networks at somewhat lower copolymer concentrations (typically 5–10 w/w %), since the hydrophilic B blocks can act as ‘bridges’ between the hydrophobic micelle cores formed by the hydrophobic A blocks.¹⁶ Recent developments have used this concept to generate gels that are responsive to temperature,^{17,18} pH,¹⁹ biochemical oxidation²⁰ or light.²¹ Amphiphilic block copolymers can undergo self-assembly to form various nanostructures in a solvent that is selective for one of the blocks.²² Wormlike block copolymer micelles have been reported,^{23,24} but these nanostructures are generally more difficult to target than spherical or vesicular phases due to their relatively narrow

phase regions.^{25,26} Despite these difficulties, Discher and co-workers²⁷ demonstrated that wormlike micelles comprising biodegradable poly(ϵ -caprolactone)-based copolymers exhibit longer circulation times compared to spherical micelles, which leads to enhanced drug delivery performance in cancer therapies. An alternative method for the generation of wormlike micelles is to use a crystallizable core-block to drive self-assembly.^{28–30} However, there are rather few literature reports describing the gelation behavior of block copolymer worms. In early pioneering work, Bates and co-workers^{23,31} reported that cross-linkable poly(ethylene oxide)-*block*-polybutadiene diblock copolymers formed gels in relatively dilute aqueous solution. Of particular relevance to the present study, Booth and co-workers found that concentrated (25%) aqueous solutions of poly(ethylene oxide)-*block*-butylene oxide diblocks formed hard gels comprising hexagonally close-packed cylindrical micelles on heating to around 40 °C.³² Similarly, a low molecular weight nonionic Pluronic copolymer apparently undergoes a sphere-to-worm transition above 40 °C in the presence of 2.0 M NaCl, although no morphological studies were undertaken to confirm this hypothesis.^{32,33} More recently, Fernandez and co-workers³⁴ conducted extensive rheological studies on a related Pluronic copolymer and also inferred a sphere-to-worm transition at around 27 °C, albeit for a relatively concentrated 20% copolymer solution. *In contrast to these prior studies, herein we report an unusual example of stimulus-responsive diblock copolymer worms that form soft gels at ambient temperature in the absence of*

Received: March 12, 2012

Published: May 14, 2012

any added electrolyte. One problem that prevents the more widespread use of self-assembled block copolymer wormlike micelles is the difficulty in preparing large batches of material at industrially relevant concentrations. Furthermore, the processing route can introduce various kinetic effects depending on the chosen pathway (e.g., solvent switch, film rehydration, etc). This is particularly true for higher molecular weight copolymers, which often form nonergodic (kinetically frozen) aggregates.²⁵

Several research groups have recently examined the use of polymerization-induced self-assembly *via* living radical polymerization,^{26,35–40} which eliminates the need for further processing steps. In principle, this is a versatile and highly efficient route to produce either diblock copolymer spheres or worms or vesicles, since the final copolymer morphology is dictated by the copolymer curvature.⁴¹ Recently, we reported using reversible addition–fragmentation chain transfer (RAFT) chemistry for the aqueous dispersion polymerization of 2-hydroxypropyl methacrylate (HPMA) using a water-soluble poly(glycerol monomethacrylate) (PGMA) macro-CTA.³⁹ In the present work, we exploit this robust formulation to generate well-defined PGMA-HPMA diblock copolymers (hereinafter denoted as G_n - H_m for brevity, where subscripts 'n' and 'm' are the mean degrees of polymerization of each block) that self-assemble *in situ* to form wormlike micelles. At a copolymer concentration of 10 w/w %, soft free-standing physical hydrogels are generated due to interworm entanglements. Moreover, thermo-reversible degelation occurs rapidly on cooling below ambient temperature due to a worm-to-sphere transition. This suggests that ultrafiltration of the cold block copolymer dispersion in its low-viscosity spherical form may offer a facile route to readily sterilizable, recyclable hydrogels for biomedical applications. This is important, because rigorous sterilization typically requires either (i) using toxic reagents such as ethylene oxide, (ii) autoclaving for extended periods at elevated temperatures, or (iii) exposure to γ radiation. Each of these routes could potentially have a deleterious effect on the copolymer (and also on any active compound within the gelling formulation).

MATERIALS AND METHODS

Materials. Glycerol monomethacrylate (GMA; 99.8%) was donated by Cognis Performance Chemicals (Hythe UK) and used without further purification. 2-Hydroxypropyl methacrylate (HPMA), 2-cyano-2-propyl dithiobenzoate (CPDB), 4,4'-azobis(4-cyanopentanoic acid) (ACVA; V-501; 99%), D_2O , anhydrous ethanol (99%) and Spectra-Por dialysis tubing (molecular weight cutoff = 1000) were purchased from Sigma-Aldrich UK and were used as received. All solvents were of HPLC quality and purchased from Fisher Scientific (Loughborough, UK). NHS-Fluorescein was purchased from Thermo Scientific and used as received. *Staphylococcus aureus* (strain Oxford) bacteria were grown in brain-heart infusion broth (Oxoid/Fisher Scientific) for 24 h to a concentration of approximately 8×10^9 bacteria/mL. The oral keratinocyte cell line H357 (kind gift from S. Prime, University of Bristol) was grown in DMEM supplemented with L-glutamine and 10% fetal calf serum overnight in 5% CO_2 at 37 °C.

COPOLYMER SYNTHESIS

Synthesis of the PGMA₅₄ macro-CTA. CPDB RAFT agent (0.80 g, 3.60 mmol) and GMA monomer (271.1 mmol, 43.42 g) were weighed into a 250 mL round-bottomed flask and purged under N_2 gas for 20 min. ACVA (202.6 mg, 0.70 mmol; CPDB/ACVA molar ratio = 5:1) and anhydrous ethanol (60.9 mL), previously purged with N_2 for 30 min, were then

added and the resulting red 40 w/w % alcoholic solution was degassed with N_2 for a further 10 min. The sealed flask was immersed into an oil bath set at 70 °C for 95 min and quenched in liquid nitrogen. Addition of methanol (100 mL) to the reaction solution was followed by precipitation into a 10-fold excess of cyclohexane (1 L). The precipitated PGMA macro-CTA was washed three times with cyclohexane, then dialyzed against methanol overnight (with three changes of methanol). ¹H NMR indicated a mean degree of polymerization of 54 for the PGMA macro-CTA. DMF GPC analysis (refractive index detector) gave $M_n = 15,400$ and $M_w/M_n = 1.13$ using a series of near-monodisperse poly(methyl methacrylate) calibration standards.

RAFT Aqueous Dispersion Polymerization of PGMA₅₄-PHPMA₁₄₀. A typical protocol for the synthesis of PGMA₅₄-PHPMA₁₄₀ is as follows: PGMA₄₇ macro-CTA (0.500 g, 0.056 mmol) and HPMA monomer (1.14 g, 7.9 mmol) were weighed into a 25 mL round-bottomed flask and purged with N_2 for 20 min. ACVA was added (5.30 mg, 0.019 mmol, CPDB/ACVA molar ratio = 3:1) and purged with N_2 for a further 5 min. Deionized water (14.8 mL), which had been purged with N_2 for 30 min, was then added, and the resulting 10 w/w % aqueous solution was degassed for a further 5 min prior to immersion in an oil bath set at 70 °C. The polymerizing solution was stirred overnight (4 h) to ensure complete HPMA monomer conversion (>99% by ¹H NMR) and quenched with exposure to air.

STERILIZATION STUDIES

Preparation of Fluorescently Labeled Bacteria. Overnight cultures of *Staphylococcus aureus* were washed in phosphate buffered saline (PBS) by centrifugation three times to remove excess culture medium. The bacteria were then resuspended in PBS, adjusted to a concentration of approximately 8×10^9 bacteria/mL and fluorescently labeled by incubating with NHS-FITC (2 μ L of a 10 mg mL⁻¹ DMF solution) for 1 h at 21 °C in the dark with gentle agitation. Excess NHS-FITC was then removed by centrifugation–redispersion cycles in PBS until the supernatant contained no fluorescence.

Sterilization via Ultrafiltration. A 10 w/w % aqueous G_{54} - H_{140} worm gel (1.0 mL) was cooled to around 4 °C in an ice bath, which caused its immediate degelation. The resulting cold free-flowing G_{54} - H_{140} aqueous dispersion was mixed with FITC-labeled bacteria (0.50 mL) with gentle agitation. This bacteria-loaded copolymer dispersion was then allowed to regel by warming to room temperature and the fluorescence measured using a plate reader (MG LabtechPolarstar Galaxy) with a 490 ± 10 nm excitation filter and 520 ± 10 nm emission filter (FITC maximum absorbance, $\lambda_{abs} = 495$ nm, maximum emission, $\lambda_{em} = 519$ nm). On cooling again to 4 °C, the resulting free-flowing bacteria/copolymer solution was ultrafiltered through a prechilled 0.45 μ m Whatman filter, then allowed to warm up to room temperature again and the fluorescence of the reformed gel measured at 520 nm. This experiment was repeated three times. For comparison, a control sample was prepared by ultrafiltering a cold aqueous G_{54} - H_{140} copolymer dispersion without bacteria at 4 °C and measuring its fluorescence, as described above. Also, an unfiltered, bacteria-loaded aqueous G_{54} - H_{140} copolymer dispersion was prepared for growth studies. To confirm that sterilization had been achieved, both the ultrafiltered and unfiltered bacteria/copolymer mixtures were inoculated into brain-heart infusion

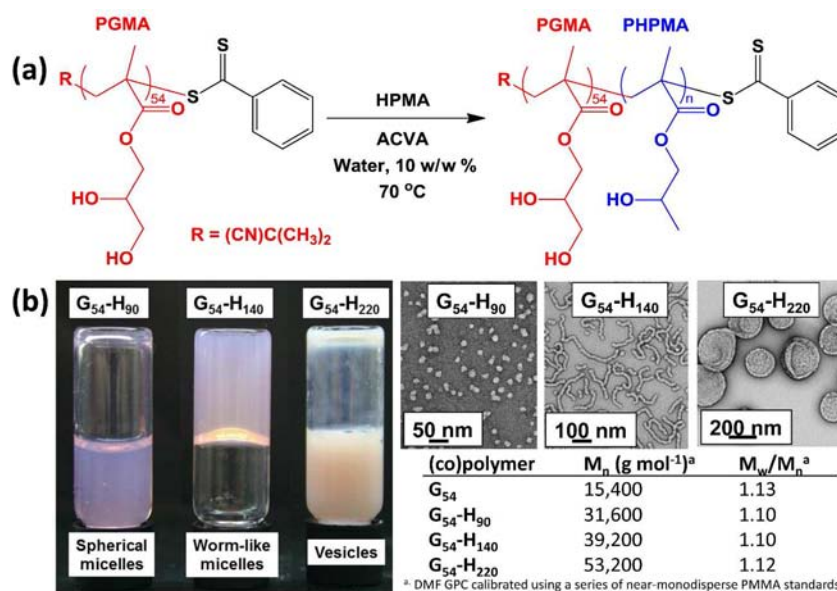


Figure 1. (a) Polymerization of HPMA monomer using a PGMA₅₄ macro-CTA under RAFT aqueous dispersion polymerization conditions at 10 w/w % and 70 °C. (b) Digital photographs recorded for three G₅₄-H_n copolymer dispersions (10 w/w %) at 21 °C, TEM images obtained for the diluted aqueous dispersions and the molecular weight data for the corresponding diblock copolymers. A self-supporting gel is formed by the wormlike micelles, as opposed to the free-flowing low-viscosity fluids formed by either spherical micelles or vesicles.

broth and cultured for 16 h at 37 °C. Broths were subsequently plated onto blood agar (Columbia agar supplemented with 5% oxalated horse blood) and incubated for 24 h at 37 °C. Bacterial growth was assessed by visual inspection of both broth and plate cultures.

■ BIOCOMPATIBILITY STUDIES

Oral keratinocytes (H357) were seeded (9×10^4 cells per well) into 24 well plates with DMEM supplemented with 0.58 mg mL⁻¹ L-glutamine and 10% fetal calf serum and grown for 72 h in 5% CO₂ at 37 °C to yield monolayers containing approximately 1.7×10^5 cells per well. Aqueous 10 w/w % G₅₄-H₁₄₀ copolymer dispersion and sterilized via ultrafiltration as described above was then supplemented with 10×-strength DMEM (Sigma) plus glutamine and fetal calf serum to prepare final copolymer gel solutions of 8.0, 6.5, 5.0, 3.5, and 2.0 w/w %. These solutions were then cooled on ice, and 450 μL of each solution was placed on top of keratinocyte monolayers. After 48 h incubation with 5% CO₂ at 37 °C, the copolymer supernatants were removed, and the extent of cell survival was assessed using the following three techniques: (i) total cell count using a hemocytometer; (ii) typan blue exclusion (0.40 w/w %) by counting the blue-stained cells; (iii) MTT assay by measuring the reduction of 0.50 mg mL⁻¹ thiazolyl blue tetrazolium blue to give a purple formazan species at 540 nm.

■ CHARACTERIZATION

NMR Spectroscopy. ¹H NMR spectra were recorded using a 500 MHz Bruker Avance-500 spectrometer (64 scans averaged per spectrum).

Gel Permeation Chromatography (GPC). Copolymer molecular weights and polydispersities were determined using a DMF GPC setup operating at 60 °C and comprising two Polymer Laboratories PL gel 5 μm Mixed-C columns connected in series to a Varian 390-LC multidetector suite (refractive index detector) and a Varian 290-LC pump injection module. The GPC eluent was HPLC grade DMF containing 10

mM LiBr at a flow rate of 1.0 mL min⁻¹. DMSO was used as a flow-rate marker. Calibration was conducted using a series of 10 near-monodisperse poly(methyl methacrylate) standards ($M_n = 625$ to 618,000 g mol⁻¹). The chromatograms were analyzed using Varian Cirrus GPC software (version 3.3).

Dynamic Light Scattering. Intensity-average hydrodynamic diameters of the dispersions were obtained by DLS (Malvern Zetasizer NanoZS instrument) using non-negative least-squares (NNLS) algorithm. Aqueous dispersions of 0.50 w/w % were analyzed using disposable cuvettes and all data were averaged over three consecutive runs.

Transmission Electron Microscopy (TEM). Aggregate solutions were diluted 50-fold at 20 °C to generate 0.20 w/w % dispersions. Copper/palladium TEM grids (Agar Scientific) were surface-coated in-house to yield a thin film of amorphous carbon. The grids were then plasma glow-discharged for 30 s to create a hydrophilic surface. Individual samples (0.20 w/w %, 12 μL) were adsorbed onto the freshly glow-discharged grids for one minute and then blotted with filter paper to remove excess solution. To stain the aggregates, uranyl formate (0.75 w/w %) solution (9 μL) was soaked on the sample-loaded grid for 20 s and then carefully blotted to remove excess stain. The grids were then dried using a vacuum hose. Imaging was performed on a Phillips CM100 instrument at 100 kV, equipped with a Gatan 1 k CCD camera. For TEM grid preparation at low temperature, all materials and samples (i.e., copolymer solution, deionized water, uranyl formate solution, freshly glow-discharged TEM grids, tweezers, filter papers, etc.) were placed in a cold room set at 4 °C and allowed to equilibrate for 20 min. The cold 10 w/w % G₅₄-H₁₄₀ solution was diluted to 0.20 w/w % with cold deionized water prior to TEM grid preparation. The grid was then stained as described above, and excess solution was removed immediately via blotting after 20 s.

Small-Angle X-ray Scattering (SAXS). SAXS measurements were performed using a Bruker AXS Nanostar instrument (Cu K_α radiation) equipped with a HiStar area

detector and a semitransparent beam-stop. SAXS patterns were recorded over a scattering vector q range of $0.01 \text{ \AA}^{-1} < q < 0.20 \text{ \AA}^{-1}$. A liquid cell comprising two mica windows (each of $25 \mu\text{m}$ thickness) separated by a polytetrafluoroethylene spacer of 1 mm thickness was used as a sample holder. SAXS studies of 10.0 w/w % aqueous copolymer solutions were conducted at both 5 and 25 °C. Two-dimensional (2D) SAXS patterns were reduced to one-dimensional (1D) profiles by a standard protocol within the Bruker Nanostar software package and were subjected to normalization and background corrections. A scattering curve for pure water $d\Sigma/d\Omega_{\text{water}} = 0.0165 \text{ cm}^{-1}$ was recorded and used as a reference for the absolute calibration of the SAXS patterns.⁴² The size and shape of the self-assembled structures have been estimated from distance distribution functions. A distance distribution function for spherical particles, $p(r)$, or a distance distribution function of a rod cross-section, $p_c(r)$ were obtained from SAXS patterns by an indirect Fourier transformation method⁴³ using a regularization technique implemented in a computer program (GNOM).⁴⁴ The parameter TOTAL calculated by the program GNOM has been used as the main criterion for the determination of the optimum value of the regularization parameter (Lagrange multiplier).⁴⁴

Rheology Studies. The storage modulus (G') and loss modulus (G'') curves for the $G_{54}\text{-H}_{140}$ diblock copolymer worm gel were determined using a TA Instruments AR-G2 rheometer equipped with a Peltier heating/cooling plate. A cone-and-plate geometry (40 mm 2° aluminum cone) was used for the measurements. Temperature sweeps were conducted at a fixed strain of 1% using an angular frequency of 10 rad s^{-1} . Sweeps were conducted at $1 \text{ }^\circ\text{C min}^{-1}$, with an equilibration time of 5 min at 2 °C.

RESULTS AND DISCUSSION

HPMA monomer was polymerized using a near-monodisperse PGMA₅₄ macro-CTA *via* RAFT aqueous dispersion polymerization to yield three well-defined, low polydispersity $G_{54}\text{-H}_n$ diblock copolymers (where $n = 90, 140$ or 220) at 10.0 w/w %, see Figure 1a,b (and also Figure S1 in Supporting Information [SI]). In each case more than 99% HPMA conversion was achieved within 2 h at 70 °C, as judged by ¹H NMR. Transmission electron microscopy (TEM) studies indicate spherical micelles for $G_{54}\text{-H}_{90}$, wormlike micelles for $G_{54}\text{-H}_{140}$ and a purely vesicular phase for $G_{54}\text{-H}_{220}$, see Figure 1b. As expected, the larger wormlike and vesicular aggregates give rise to turbid dispersions due to their stronger light scattering characteristics (see Figure 1b).

The stirred wormlike micelle dispersion remains fluid at 70 °C, but forms a soft free-standing physical gel on standing for 16 h at 21 °C (see Figure 1b). Gelation is due to interworm entanglements, as found for wormlike surfactant micelles.⁷ In contrast, the spherical and vesicular dispersions remain free-flowing, low-viscosity fluids.

Somewhat counterintuitively, rheological studies confirm that a 10 w/w % aqueous $G_{54}\text{-H}_{140}$ wormlike copolymer gel undergoes *degelation on cooling* (see Figure 2a).^{18,45} This thermal transition is reversible, and some hysteresis is observed, as expected for a first-order phase transition. The storage modulus (G') exceeds the loss modulus (G'') at 21 °C, indicating the formation of a visco-elastic gel. However, at 14 °C, the G' and G'' curves cross over, resulting in a reduction in G' by 2 orders of magnitude and a free-flowing fluid. This fluid was held at 2 °C for 5 min and then heated back to 25 °C. The

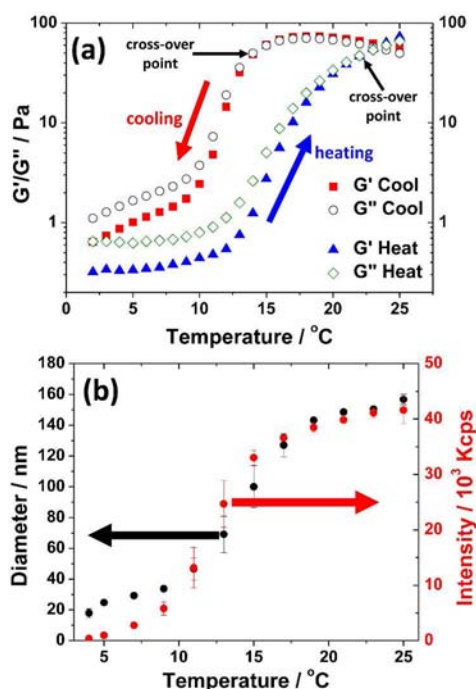


Figure 2. (a) Variation of storage moduli (G' , filled symbols) and loss moduli (G'' , open symbols) for a $G_{54}\text{-H}_{140}$ wormlike micelle gel at 10 w/w % during temperature cycling at $1 \text{ }^\circ\text{C min}^{-1}$: (i) cooling from 25 to 2 °C ($G' =$ filled red squares, $G'' =$ open black circles) and (ii) subsequent warming from 2 to 25 °C ($G' =$ filled blue triangles, $G'' =$ open green diamonds). (b) Temperature-dependent intensity-average diameter and scattered light intensity determined by DLS for the same PGMA₅₄-PHPMA₁₄₀ wormlike dispersion diluted to 0.50 w/w % (i.e., below its critical gelation concentration of around 5%).

critical regelation temperature (i.e., where $G' > G''$) was 22 °C and the final G' of around 90 Pa was comparable to the initial value. This hysteresis may also indicate the time scale required for interworm entanglements at this concentration. Further studies (data not shown) indicate that these gels are shear-thinning, suggesting that magnetic stirring during RAFT polymerization provides sufficient shear to inhibit gelation at 70 °C. A full rheological study of these gels will be published elsewhere in due course.

In order to examine the degelation mechanism, temperature-dependent dynamic light scattering (DLS) studies were conducted on a 0.50 w/w % $G_{54}\text{-H}_{140}$ wormlike micelle solution (see Figure 2b). Above 20 °C, an apparent *sphere-equivalent* hydrodynamic diameter of around 150 nm is observed, which is consistent with the presence of wormlike micelles. However, cooling this dilute dispersion results in a monotonic reduction in both particle size and scattered light intensity (I_{scat}), with 30 nm 'nano-objects' being observed below 10 °C. This dramatic decrease in hydrodynamic diameter (Figure 2b) correlates well with a significant reduction in G' and G'' moduli (Figure 2a) observed over the same temperature range. In principle, there are three possible mechanisms for degelation: (i) worm disentanglement, (ii) worm dissolution into individual copolymer chains, and (iii) worms undergoing a change in morphology. While the first hypothesis is consistent with the rheology measurements, worm disentanglements alone should not result in the significant size reduction observed by DLS. Complete dissolution of the worms can also be ruled out, as the hydrodynamic diameter observed at 4 °C is still

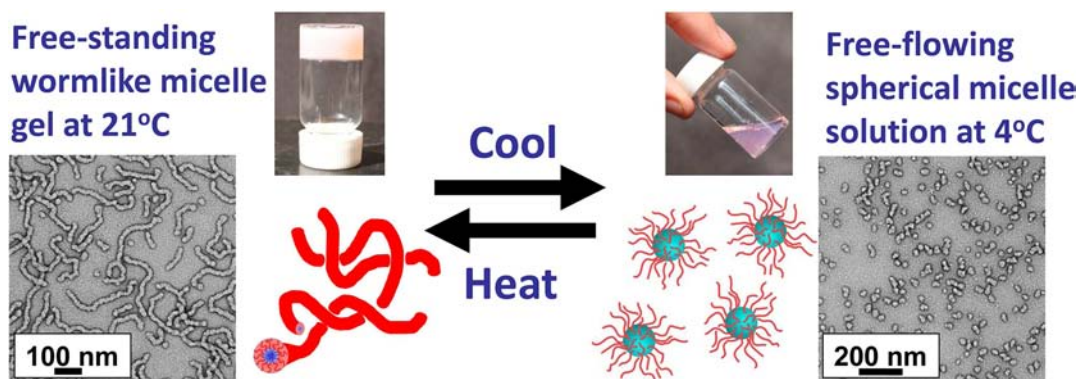


Figure 3. Thermoresponsive aqueous solution behavior of a 10 w/w % aqueous dispersion of G_{54} - H_{140} diblock copolymer particles. A free-standing gel is formed at 21 °C, which becomes a free-flowing solution when cooled below 10 °C. TEM studies of grids prepared from a dilute aqueous dispersion of G_{54} - H_{140} dried at either 21 or 4 °C provide strong evidence for a reversible worm-to-sphere transition.

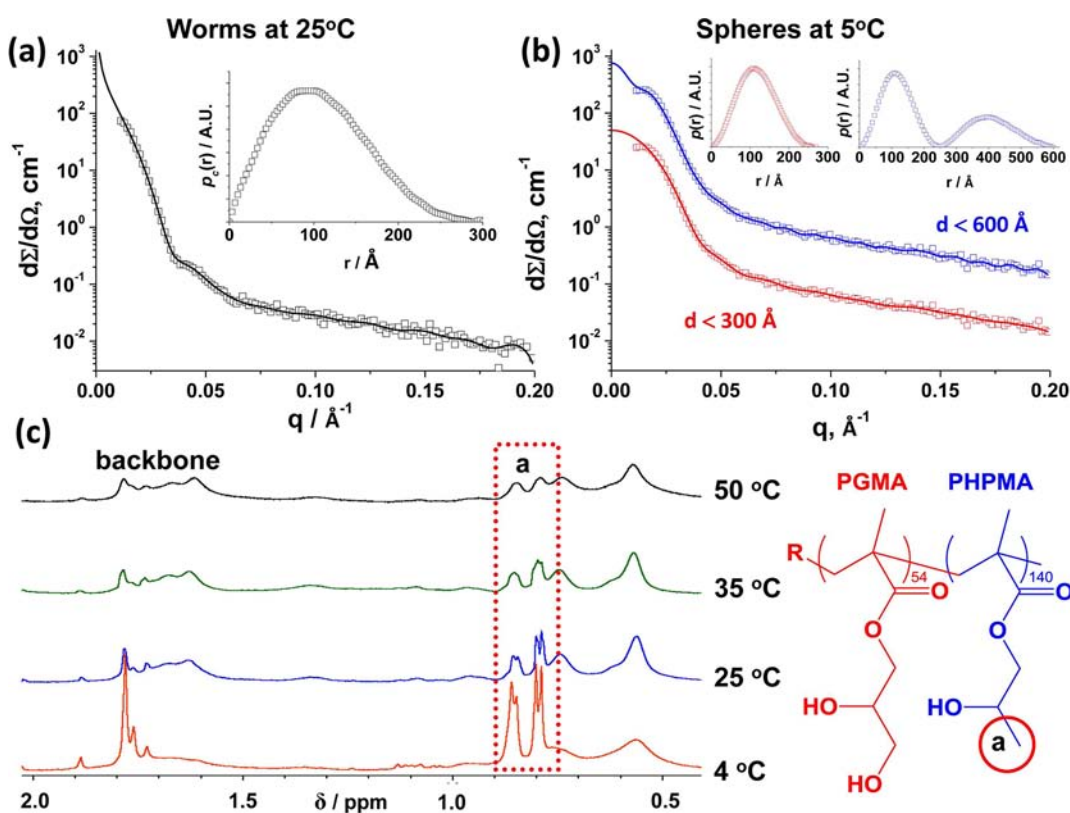


Figure 4. SAXS patterns (differential cross section, $d\Sigma/d\Omega$, versus scattering vector, q) and the corresponding distance distribution functions, $p_c(r)$ or $p(r)$, (see insets) obtained for a 10 w/w % aqueous dispersion of G_{54} - H_{140} diblock copolymer at (a) 25 °C and (b) 5 °C. For the lower temperature, two $p(r)$ calculations are presented whereby $p(r)$ is assumed to be nonzero for either $0 < r < 300$ Å (red squares) or for $0 < r < 600$ Å (blue squares). The first model is consistent with the formation of spherical particles, whereas the latter model (the corresponding SAXS pattern is multiplied by ten for clarity) suggests spherical dimers (and provides a better correlation with the SAXS data, especially the inflection at low q). (c) Partial 500 MHz ^1H NMR spectra recorded for a 10 w/w % aqueous G_{54} - H_{140} diblock copolymer dispersion at 4, 25, 35, and 50 °C (using minimal D_2O as a signal lock). All spectra were normalized relative to signal 'a'. The PHPMA signals become more intense on cooling, indicating greater hydration of the core-forming block at lower temperature.

somewhat larger than expected for individual copolymer chains. The third hypothesis is actually correct, as confirmed by the following observations.

A dilute aqueous dispersion of G_{54} - H_{140} was rapidly dried onto transmission electron microscopy (TEM) grids at either 21 or 4 °C to ensure that the original copolymer morphology is preserved in each case (see Materials and Methods section). TEM studies of these grids indicated a significant change in morphology from anisotropic worms at 21 °C to pseudospher-

ical micelles (spheres plus spherical dimers) at 4 °C (see Figure 3). Since the latter particles cannot form entanglements, it follows that the mechanism for macroscopic degelation on cooling must be a thermoreversible worm-to-sphere transition.

Small angle X-ray scattering was utilized to characterize a 10 w/w % G_{54} - H_{140} aqueous copolymer dispersion at both 25 and 5 °C (see Figure 4). This worm-to-sphere transition leads to significant changes in the SAXS data (see Figure 4 and Figure S2, SI). Compared to the SAXS pattern recorded for spheres at

5 °C, the SAXS pattern observed at 25 °C for the wormlike micelles has a relatively high intensity in the Guinier region ($q < 0.02 \text{ \AA}^{-1}$) and a relatively low intensity at high q (see Figure S2, SI). As the wormlike micelles are approximately cylindrical in shape, the enhanced intensity at low q is associated with a change in slope of the SAXS pattern in the Guinier region from zero (as expected for uniform spheres) to -1 (which is characteristic for cylindrical rods). Assuming that the aqueous dispersion is a two-phase system and that the volume fractions of the two components in the sample remain constant during the worm-to-sphere transition, the observed change in overall intensity should not affect the invariant [$Q = \int_0^\infty d\Sigma / d\Omega(q) q^2 dq$]. This is indeed the case: integrating throughout reciprocal space confirms that the overall scattering power of the sample remains virtually constant after the order–order transition ($Q = 0.17 \pm 0.01 \text{ cm}^{-1} \text{ \AA}^{-3}$ at 5 °C and $Q = 0.15 \pm 0.01 \text{ cm}^{-1} \text{ \AA}^{-3}$ at 25 °C). The apparent reduction in Q at 25 °C is (just) within experimental error. If this small difference is real, it may be due to the thermal expansion of the sample, which would reduce the electron density difference between the copolymer and water. The pronounced shoulder observed in the SAXS pattern for the wormlike micelles at $q \approx 0.05 \text{ \AA}^{-1}$ (see Figure 4a) is associated with the form factor expected for cylinders (see the simulated SAXS curve in Figure S2, SI). However, the spherical micelle SAXS pattern shown in Figure 4b is a featureless smooth curve, corresponding to the form factor associated with highly polydisperse spheres and/or pseudospherical particles (see TEM images in Figure 3). In this case analysis of the pair-distance distribution function, $p(r)$, which represents real space, is a more effective tool to estimate the size and shape of the nano-objects. The distance distribution function of the wormlike micelle cross-section, $p_c(r)$, calculated from the SAXS pattern recorded at 25 °C (Figure 4a) assuming rodlike micelles (job 4 in GNOM software) and $r < 300 \text{ \AA}$, approaches zero at approximately 250 Å (Figure 4a, inset). This cross-section, which corresponds to the maximum worm diameter, is in good agreement with the TEM studies (Figure 3, left-hand image). The scattering intensities recalculated from the $p_c(r)$ data provide a good fit to the experimental SAXS pattern (Figure 4a, solid line). The distance distribution function calculated from the SAXS pattern recorded at 5 °C (Figure 4b) assuming a globular shape and $r < 300 \text{ \AA}$ yields a bell-shaped profile for which $p(r)$ approaches zero above approximately 250 Å. This value corresponds to the maximum spherical micelle diameter, which is again in good agreement with the TEM data (Figure 3, right-hand image). The scattering intensities recalculated from the $p(r)$ provide a satisfactory fit to the experimental pattern (Figure 4b, red solid line). However, an even better correlation between the recalculated SAXS data and that obtained experimentally at 5 °C can be achieved by assuming a *significantly larger* interval, $r < 600 \text{ \AA}$ (Figure 4b, blue solid line). In this refinement, the new $p(r)$ profile (Figure 4b, blue squares) with an oscillation corresponding to two-domain particles suggests that either the spherical micelles are actually *spherical dimers* or that the relatively high particle concentration (10 w/w %) causes interparticle interference. However, close inspection of TEM images (see Figure 3) provides good evidence for the formation of a significant proportion of *spherical dimers*. Moreover, SAXS studies during thermal cycling confirm that this worm-to-sphere transition exhibits excellent reversibility and reproducibility (see Figure S2 in SI).

To probe the molecular origin of the worm-to-sphere transition, variable-temperature ^1H NMR spectroscopy was utilized to assess a 10 w/w % dispersion of $\text{G}_{54}\text{-H}_{140}$ particles in D_2O (see Figure 4c). The PHPMA signals at around 0.80–0.90 ppm due to the pendent methyl group become much more intense at lower temperature, indicating a greater degree of hydration for these core-forming chains. This increases their mobility and reduces the interfacial tension between the two blocks. This increases the copolymer curvature, which in turn favors the formation of spherical micelles at lower temperature, hence inducing the worm-to-sphere transition.

In principle, this order-order transition can be exploited for potential biomedical applications. Thus, cooling a 10 w/w % aqueous dispersion of the $\text{G}_{54}\text{-H}_{140}$ copolymer worms to 4 °C produced a low-viscosity fluid comprising pseudospherical nanoparticles. To establish proof-of-concept, this cold free-flowing dispersion was deliberately contaminated with 4×10^9 FITC-labeled *S. aureus* bacteria at 4 °C, and regelation occurred on warming to room temperature, as expected. Subsequently, this bacteria-loaded $\text{G}_{54}\text{-H}_{140}$ copolymer sample was readily sterilized by cooling to 4 °C to produce a free-flowing fluid once again, followed by ultrafiltration through a 0.45 μm membrane filter. This protocol efficiently removes the micrometer-sized bacteria, but allows passage of the low-viscosity copolymer nanoparticles through the pores. The bacteria-loaded copolymer worm gel exhibited strong fluorescence at 520 nm, whereas negligible fluorescence (i.e., comparable to that of a control copolymer gel not contaminated with bacteria) was observed for the reformed sterile copolymer gel obtained after ultrafiltration (see Figure 5a). Finally, both the ultrafiltered (bacteria-free) and unfiltered (bacteria-loaded) copolymer gels were cultured for 24 h at 37 °C to verify complete removal of bacteria. Figure 5b shows substantial bacterial growth from the unfiltered copolymer gel, whereas the ultrafiltered copolymer gel shows no growth at all, thus confirming that low-temperature ultrafiltration provides a facile route to sterile copolymer gels, as anticipated.

The biocompatibility of the worm gel was assessed by placing 2–8% $\text{G}_{54}\text{-H}_{140}$ copolymer solutions onto monolayer cultures of epithelial keratinocytes. Cell viabilities were assessed after 48 h using a colorimetric assay, which relies on MTT reduction by the mitochondrial dehydrogenase produced by viable cells. Figure S3 (see SI) suggests only a slight reduction in cell viability over this time frame, with cell viabilities remaining above 92% after 48 h for diblock copolymer concentrations between 2.0, 3.5, 5.0, 6.5, and 8.0 w/w %. Also, cell death was assessed by the uptake of Trypan blue dye, which cannot cross live cell membranes. A modest increase in the blue cell (dead cell) count indicated only a marginally greater cell death (7.7%) over 48 h, as compared to the 5.0% cell death observed for the control experiments conducted in the absence of any copolymer.

Certain conventional surfactants are also known to form wormlike micellar gels that respond to changes in either pH^{10} or temperature,¹¹ with worm-to-sphere transitions being invoked to explain this behavior. However, such surfactant gels are not suitable for biomedical applications. Similarly, a commercially available $\text{PEO}_{19}\text{-PPO}_{43}\text{-PEO}_{19}$ triblock copolymer undergoes a sol–gel transition that is apparently due to a sphere-to-worm transition on heating above 30 °C.³³ However, in the latter case gelation only occurs in the presence of 2.0 M NaCl, which does not correspond to physiological conditions. In contrast, given the commercial availability of the methacrylic

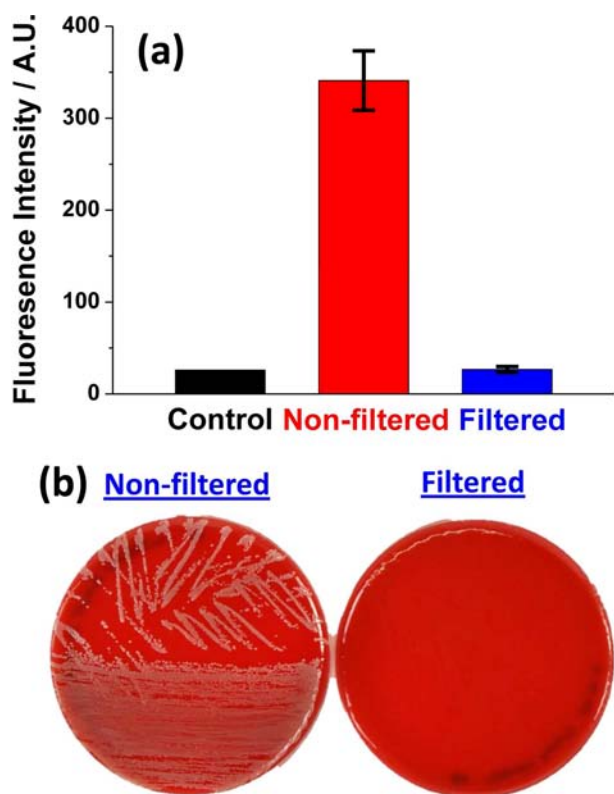


Figure 5. Sterilization of copolymer worm gels by cold ultrafiltration. (a) Fluorescence observed before and after ultrafiltration of $G_{54}\text{-}H_{140}$ diblock copolymer after its deliberate contamination with FITC-labeled *S. aureus*. As expected, the unfiltered bacteria-loaded $G_{54}\text{-}H_{140}$ copolymer gel exhibits strong fluorescence (red column) relative to the bacteria-free copolymer control (black column). On cooling to 4 °C, this gel becomes a free-flowing, low-viscosity fluid; under these conditions the fluorescent micrometer-sized bacteria are efficiently removed from the block copolymer nanoparticles by ultrafiltration (blue column). (b) Plate cultures of unfiltered and ultrafiltered copolymer gels obtained after incubation for 24 h at 37 °C. Clearly, substantial bacterial growth has occurred in the unfiltered copolymer gel. In contrast, no bacterial growth is observed for the ultrafiltered copolymer gel (right-hand image), indicating complete removal of *S. aureus*. The images are representative of triplicate experiments. The fluorescence values are means (\pm s.d.) of triplicate experiments.

monomers, the efficient, scalable, one-pot polymerization protocol, and the facile sterilization protocol, these novel copolymer worm gels appear to be promising for a range of biomedical applications, including injectable scaffolds for stem cell growth.^{14,46} This possibility will be explored in future work.

CONCLUSIONS

In summary, a biocompatible thermoresponsive diblock copolymer self-assembles in aqueous solution to give wormlike particles that form a soft, free-standing physical hydrogel at (or above) ambient temperature. On cooling to 4 °C, transmission electron microscopy and small-angle X-ray scattering studies confirm that the wormlike particles form spheres, causing immediate degelation. Since this worm-to-sphere transition is fully reversible, it offers a highly convenient route to sterilizable gels: micrometer-sized fluorescently labeled bacteria deliberately introduced into the gel are completely removed on ultrafiltration of the low-viscosity spherical nanoparticles at 4 °C.

ASSOCIATED CONTENT

Supporting Information

DMF GPC traces of the PGMA-PPMA diblock copolymers, SAXS patterns confirming reversibility of the worm-to-sphere transition, and MTT cytotoxicity data. This material is available free of charge via the Internet at <http://pubs.acs.org>

AUTHOR INFORMATION

Corresponding Author

s.p.armes@sheffield.ac.uk

Notes

The authors declare no competing financial interest.

ACKNOWLEDGMENTS

S.P.A. and A.J.R. thank EPSRC for postdoctoral support of A.B. (Platform Grants EP/E012949/1 and EP/J007846/1). R.B. thanks the University of Sheffield for a summer studentship. C.W.I.D. thanks Brenka McCabe for help with the biocompatibility assays.

REFERENCES

- (1) Peppas, N. A.; Hilt, J. Z.; Khademhosseini, A.; Langer, R. *Adv. Mater.* **2006**, *18*, 1345–1360.
- (2) Banwell, E. F.; Abelardo, E. S.; Adams, D. J.; Birchall, M. A.; Corrigan, A.; Donald, A. M.; Kirkland, M.; Serpell, L. C.; Butler, M. F.; Woolfson, D. N. *Nat. Mater.* **2009**, *8*, 596–600.
- (3) Wichterle, O.; Lim, D. *Nature* **1960**, *185*, 117–118.
- (4) Silva, G. A.; Czeisler, C.; Niece, K. L.; Beniash, E.; Harrington, D. A.; Kessler, J. A.; Stupp, S. I. *Science* **2004**, *303*, 1352–1355.
- (5) Weber, K.; Osborn, M. *J. Biol. Chem.* **1969**, *244*, 4406–8.
- (6) He, C. L.; Kim, S. W.; Lee, D. S. *J. Controlled Release* **2008**, *127*, 189–207.
- (7) Dreiss, C. A. *Soft Matter* **2007**, *3*, 956–970.
- (8) Kopecek, J.; Yang, J. Y. *Acta Biomater.* **2009**, *5*, 805–816.
- (9) Adams, D. J.; Topham, P. D. *Soft Matter* **2010**, *6*, 3707–3721.
- (10) Chu, Z. L.; Feng, Y. J. *Chem. Commun.* **2010**, *46*, 9028–9030.
- (11) Chu, Z. L.; Feng, Y. J. *Chem. Commun.* **2011**, *47*, 7191–7193.
- (12) Aggeli, A.; Bell, M.; Boden, N.; Keen, J. N.; Knowles, P. F.; McLeish, T. C. B.; Pitkeathly, M.; Radford, S. E. *Nature* **1997**, *386*, 259–262.
- (13) Nowak, A. P.; Breedveld, V.; Pakstis, L.; Ozbas, B.; Pine, D. J.; Pochan, D.; Deming, T. J. *Nature* **2002**, *417*, 424–428.
- (14) Haines-Butterick, L.; Rajagopal, K.; Branco, M.; Salick, D.; Rughani, R.; Pilarz, M.; Lamm, M. S.; Pochan, D. J.; Schneider, J. P. *Proc. Natl. Acad. Sci. U.S.A.* **2007**, *104*, 7791–7796.
- (15) Jeong, B.; Bae, Y. H.; Lee, D. S.; Kim, S. W. *Nature* **1997**, *388*, 860–862.
- (16) Tsitsilianis, C. *Soft Matter* **2010**, *6*, 2372–2388.
- (17) Li, C. M.; Tang, Y. Q.; Armes, S. P.; Morris, C. J.; Rose, S. F.; Lloyd, A. W.; Lewis, A. L. *Biomacromolecules* **2005**, *6*, 994–999.
- (18) Madsen, J.; Armes, S. P.; Lewis, A. L. *Macromolecules* **2006**, *39*, 7455–7457.
- (19) Ma, Y. H.; Tang, Y. Q.; Billingham, N. C.; Armes, S. P.; Lewis, A. L. *Biomacromolecules* **2003**, *4*, 864–868.
- (20) Li, C. M.; Madsen, J.; Armes, S. P.; Lewis, A. L. *Angew. Chem., Int. Ed.* **2006**, *45*, 3510–3513.
- (21) Woodcock, J. W.; Wright, R. A. E.; Jiang, X. G.; O'Lenick, T. G.; Zhao, B. *Soft Matter* **2010**, *6*, 3325–3336.
- (22) Zhang, L. F.; Eisenberg, A. *Science* **1995**, *268*, 1728–1731.
- (23) Won, Y. Y.; Davis, H. T.; Bates, F. S. *Science* **1999**, *283*, 960–963.
- (24) Qian, J. S.; Zhang, M.; Manners, I.; Winnik, M. A. *Trends Biotechnol.* **2010**, *28*, 84–92.
- (25) Jain, S.; Bates, F. S. *Macromolecules* **2004**, *37*, 1511–1523.
- (26) Sugihara, S.; Blanz, A.; Armes, S. P.; Ryan, A. J.; Lewis, A. L. *J. Am. Chem. Soc.* **2011**, *133*, 15707–15713.

- (27) Geng, Y.; Dalhaimer, P.; Cai, S. S.; Tsai, R.; Tewari, M.; Minko, T.; Discher, D. E. *Nat. Nanotechnol.* **2007**, *2*, 249–255.
- (28) Wang, X. S.; Guerin, G.; Wang, H.; Wang, Y. S.; Manners, I.; Winnik, M. A. *Science* **2007**, *317*, 644–647.
- (29) Gädt, T.; Jeong, N. S.; Cambridge, G.; Winnik, M. A.; Manners, I. *Nat. Mater.* **2009**, *8*, 144–150.
- (30) Petzetakis, N.; Dove, A. P.; O'Reilly, R. K. *Chem. Sci.* **2011**, *2*, 955–960.
- (31) Won, Y. Y.; Paso, K.; Davis, H. T.; Bates, F. S. *J. Phys. Chem. B* **2001**, *105*, 8302–8311.
- (32) Waton, G.; Michels, B.; Steyer, A.; Schosseler, F. *Macromolecules* **2004**, *37*, 2313–2321.
- (33) Duval, M.; Waton, G.; Schosseler, F. *Langmuir* **2005**, *21*, 4904–4911.
- (34) Fernandez, V. V. A.; Tepale, N.; Alvarez, J. G.; Perez-Lopez, J. H.; Macias, E. R.; Bautista, F.; Pignon, F.; Rharbi, Y.; Gamez-Corrales, R.; Manero, O.; Puig, J. E.; Soltero, J. F. A. *J. Colloid Interface Sci.* **2009**, *336*, 842–849.
- (35) Boisse, S.; Rieger, J.; Belal, K.; Di-Cicco, A.; Beaunier, P.; Li, M. H.; Charleux, B. *Chem. Commun.* **2010**, *46*, 1950–1952.
- (36) Zhang, X. W.; Boisse, S.; Zhang, W. J.; Beaunier, P.; D'Agosto, F.; Rieger, J.; Charleux, B. *Macromolecules* **2011**, *44*, 4149–4158.
- (37) He, W.-D.; Sun, X.-L.; Wan, W.-M.; Pan, C.-Y. *Macromolecules* **2011**, *44*, 3358–3365.
- (38) Li, Y.; Armes, S. P. *Angew. Chem., Int. Ed.* **2010**, *49*, 4042–4046.
- (39) Blanazs, A.; Madsen, J.; Battaglia, G.; Ryan, A. J.; Armes, S. P. *J. Am. Chem. Soc.* **2011**, *133*, 16581–16587.
- (40) Groison, E.; Brusseau, S.; D'Agosto, F.; Magnet, S.; Inoubli, R.; Couvreur, L.; Charleux, B. *ACS Macro Letters* **2011**, *1*, 47–51.
- (41) Blanazs, A.; Armes, S. P.; Ryan, A. J. *Macromol. Rapid Commun.* **2009**, *30*, 267–277.
- (42) Dreiss, C. A.; Jack, K. S.; Parker, A. P. *J. Appl. Crystallogr.* **2006**, *V39*, 32–38.
- (43) Glatter, O. J. *J. Appl. Crystallogr.* **1977**, *10*, 415–421.
- (44) Svergun, D. I. *J. Appl. Crystallogr.* **1992**, *25*, 495–503.
- (45) Madsen, J.; Armes, S. P.; Bertal, K.; Lomas, H.; MacNeil, S.; Lewis, A. L. *Biomacromolecules* **2008**, *9*, 2265–2275.
- (46) Bakota, E. L.; Wang, Y.; Danesh, F. R.; Hartgerink, J. D. *Biomacromolecules* **2011**, *12*, 1651–1657.